Extraction of VLSI Multiconductor Transmission Line Parameters by Complementarity

Ruben Specogna, *Member, IEEE*

***Abstract*— Solving lossy multiconductor transmission line (MTL) equations is of fundamental importance for the design and signal integrity verification of interconnections in VLSI systems. It is well established that the critical issue is the efficient and accurate electrical characterization of the MTLs through the determination of their per-unit-length parameters. In this respect, the so-called complementarity has the potential to become a fast and accurate method for the extraction of these parameters. Besides the value of the parameters, in fact, complementarity provides rigorous error bounds for them. Despite this important feature, commercial software do not use complementarity yet, due to the fact that there are unsolved theoretical issues related to the nonstandard formulation based on the electric vector potential. Some attempts to fill this gap have been already reported. The aim of this paper is to fill this gap by introducing a general formulation based on the electric vector potential highlighting the advantages of complementarity with respect to the standard first- and second-order finite element formulations.**

***Index Terms*— Complementarity, electromagnetic compatibility, multiconductor transmission lines (MTLs), parameter extraction, per-unit-length interconnections, VLSI interconnections.**

I. Introduction

THE ACCURATE computation of per-unit-length (p.u.l.) circuit parameters is the first and most critical step for a multiconductor transmission line (MTL) analysis [1]. Electromagnetic solvers play a fundamental role in the extraction of the p.u.l. parameters when the geometry is too complicated to obtain closed-form expressions. Particularly frequent are the cases of multilayered media with different material constants and "floating" conductors. Also, the efficiency of parameter extraction becomes critical, for example, when analyzing the impact of process-induced variations in VLSI interconnections [2].

In spite of the great variety of techniques proposed in the literature [1], [3], comprising the method of moments, finite differences, finite element methods (FEMs), and boundary element methods, the so-called complementarity [4]–[8] is less explored. Complementarity requires solving each electromagnetic problem two times employing a pair of formulations that provide certain upper and lower bounds for the circuit parameters [4]–[8]. Complementarity may be used also as a natural error estimator for mesh adaptivity [8]. For 2-D problems, the cheapest method to exploit complementarity involve the use of a pair of formulations based on complementary potentials, namely, the scalar potential and the vector potential [9], [10]. Without losing generality, for the exposition, we focus on stationary conduction problems for conductance matrix extraction, since, as discussed in [10], the same code may be used to solve electrostatic or magnetostatic problems to extract capacitance and inductance matrices, respectively, just by changing the material parameters.

While the FEM formulation based on the electric scalar potential is standard [11] and will not be described in this paper, the one based on an electric vector potential has been mainly considered in [9], [10], and [12]. We note that this formulation is currently not implemented in any commercial software and not routinely used even in state-of-the-art research software. This is probably due to the fact that in these references the potential design has not been considered in detail. This gap has been recently filled in [13], where a novel definition of potentials has been introduced.

The aim of this paper is to adapt the electric vector potential formulation presented in [13] to 2-D problems. Moreover, the definition of potentials is improved with respect to [13] considering also the case of perfectly insulating cavities that may be present inside the computational domain. This is quite important because not considering the proposed modifications leads to wrong results (in most cases without any warning). Finally, a novel algorithm is presented to effectively design the potentials. The algorithm is automatic and provably general, exhibits a linear worst-case computational complexity, and generalizes easily to 3-D problems. Furthermore, the algorithm is optimal in the sense that it provides the minimization of the fill-in of the linear system of equation sparse matrix.

The rest of this paper is structured as follows. In Section II, the geometric formulation for stationary conduction based on an electric vector potential is presented. In Section III, we show how the automatic generation of the so-called thick links can be performed. Section IV is devoted to the presentation of the numerical results, while, in Section V, the conclusions are drawn.

II. 2-D Vector Potential Geometric Formulation

Let us consider as the computational domain Ω for the stationary conduction problem a connected subset of the 2-D Euclidean space. Ω is represented in practice by a

Manuscript received April 20, 2012; revised September 20, 2012; accepted December 2, 2012. Date of publication January 17, 2013; date of current version December 20, 2013. This work was supported in part by the Italian Ministry of Education, University and Research under Project PRIN 2009LTRYRE.

The author is with the Dipartimento di Ingegneria Elettrica, Gestionale e Meccanica, Università di Udine, Udine I-33100, Italy (e-mail: ruben.specogna@uniud.it).

Color versions of one or more of the figures in this paper are available online at http://ieeexplore.ieee.org.

Digital Object Identifier 10.1109/TVLSI.2012.2232320

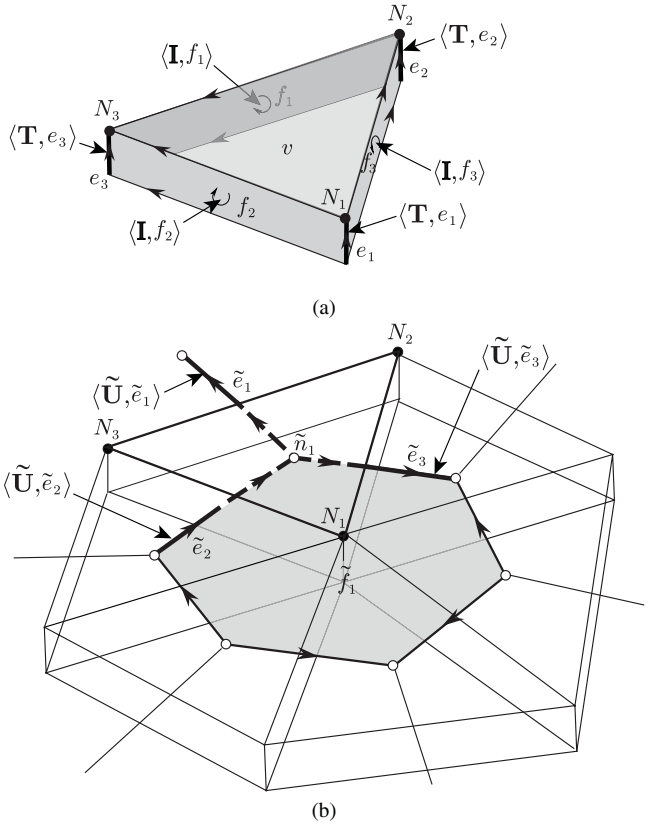

Fig. 1. Association of the physical variables to geometric elements. (a) Primal complex. (b) Dual complex.

computer aided design (CAD) model representing the real geometry of the circuit one aims to model. By importing the CAD model into any mesh generator such as GMSH (http://geuz.org/gmsh/) or RETICULA [14], it is possible to easily cover Ω by a triangular mesh. The output of the mesh generator is the mesh represented by N nodes $\{N_i\}_{i=1}^{N}$, E edges $\{E_i\}_{i=1}^{E}$, and T triangles $\{T_i\}_{i=1}^{T}$.

From the mesh, the primal cell complex $\mathcal{K}$ [15]–[17], is constructed as follows (Fig. 1). The elements are defined as rectangular prisms $\{v_i\}_{i=1}^{T}$ constructed by considering the triangles with a unit thickness [Fig. 1(a)]. Faces $\{f_i\}_{i=1}^{E}$ are the lateral faces of the prisms (one-to-one with the mesh edges), and edges $\{e_i\}_{i=1}^{N}$ are those normal to the symmetry plane (one-to-one with the mesh nodes) [Fig. 1(a)]. Then, the dual nodes $\tilde{n}$, dual edges $\tilde{e}$, and dual faces $\tilde{f}$ belonging to the dual complex $\tilde{\mathcal{K}}$ are constructed. They are obtained from $\mathcal{K}$ with the standard barycentric subdivision [15]–[17], [18, Sec. 3] [Fig. 1(b)]. Interconnections of the geometric elements of the primal and dual complex are given in terms of usual incidence matrices. We consider the incidence matrices $\mathbf{C}$ between pairs (f, e) and $\tilde{\mathbf{C}}$ between pairs $(\tilde{f}, \tilde{e})$, in regard to which $\tilde{\mathbf{C}} = \mathbf{C}^T$ holds [17], and the incidence matrix $\mathbf{D}$ between pairs (v, f). We stress that there is no need to construct the dual complex in the practical implementation, but it is required for the theoretical presentation of the formulation.

Apart from the geometry of the problem encoded in the mesh, the user has to describe the locations of electrodes, insulating cavities, and the value of current or voltage excitation for each electrode. This is performed by assigning appropriate boundary conditions. The boundary $\partial\mathcal{K}$ of the domain is formed by the connected components which model the boundaries of the cavities in $\mathcal{K}$ and by the external boundary that encircles all the cavities. The cavities in $\mathcal{K}$ represent whether the equipotential surface of perfect conductors[1] or the surface of perfect insulators[2] placed inside the domain Ω. On the external boundary, some equipotential electrodes (at least one) are posed, which are by definition disjoint and connected. The electrodes on the external boundary together with the ones corresponding to the boundaries of internal conductors are denoted as $\{\mathcal{E}_i\}_{i=0}^{N_e}$, where $N_e + 1$ is the total number of electrodes. The first element, $\mathcal{E}_0$, is referred to as reference electrode. To enforce a consistent excitation for the problem, it is usual to fix N_e independent nonlocal quantities. In practice, the typical situation is to fix for each ith electrode its potential difference with respect to the reference electrode U_e^i or alternatively—in case of a current-driven electrode[3]—the current I_e^i flowing through the electrode.

In order to formulate the problem by using the complementary geometric formulation, the following arrays of degrees of freedom (DoFs) denoted in boldface type are introduced.

1) Electric current $\mathbf{I}$, whose entries are the currents flowing through primal faces $\{f_i\}_{i=1}^{E} \in \mathcal{K}$.
2) Voltage $\tilde{\mathbf{U}}$, whose entries are the voltages on dual edges $\{\tilde{e}_i\}_{i=1}^{E} \in \tilde{\mathcal{K}}$.
3) Electric vector potential $\mathbf{T}$, whose entries are the values of the potential on primal edges $\{e_i\}_{i=1}^{N} \in \mathcal{K}$.

We denote as $\langle \mathbf{I}, f \rangle$ the current flowing through the face f [Fig. 1(a)]. With the same notation, $\langle \mathbf{T}, e \rangle$ is the electric vector potential on the edge e and $\langle \tilde{\mathbf{U}}, \tilde{e} \rangle$ is the voltage on the dual edge $\tilde{e}$ [Fig. 1(a) and (b)].

The DoF arrays are subject to constraints due to Maxwell's laws. First of all, $\mathbf{I}$ has to verify the discrete current continuity law enforced on each element $\{v_i\}_{i=1}^{T}$

$$\mathbf{DI} = \mathbf{0}. \tag{1}$$

The considered formulation requires (1) to hold implicitly by defining the potentials appropriately. This is addressed in what follows, employing, where necessary, definitions and results of algebraic topology. The reader not familiar with this topic is invited to consult any mathematical textbook such as [16] or, for an elementary uninformal introduction for engineers, [13], [18]–[20].

A. Potential Design

Let us assume for the moment that there are no cavities inside the computational domain representing perfect

[1]It is customary not to mesh the interior of perfect conductors contained in the simulation domain since the electric field inside them is known to be zero beforehand. Since the surface of each conductor is equipotential, a Dirichlet boundary condition is applied on their boundaries.

[2]It is customary not to mesh the interior of perfect insulators contained in the simulation domain since the current density field inside them is known to be zero beforehand. Since the current cannot flow through the surface of insulators, a homogeneous Neumann boundary condition is applied on their boundaries.

[3]A floating electrode is a particular case of current-driven electrode whose current is fixed to zero.

insulators (we remove this assumption in Section II-C). Thanks to the fact that $\mathbf{DC} = \mathbf{0}$ [16], [17], $\mathbf{T}$ may be defined simply with $\mathbf{I} = \mathbf{CT}$. In this way, the local current continuity law (1) holds using the potential $\mathbf{T}$. Nonetheless, this leads to an inconsistency in general. To intuitively see this fact, let us apply the current continuity law not on the boundary of exactly one element as (1), but on a 2-cycle s made by a set of faces belonging to $\mathcal{K}$. Since $\mathbf{DC} = \mathbf{0}$ holds and $\partial s = 0$ (the two-chain s is a 2-cycle by hypothesis), we have that the current through s is zero: $\langle \mathbf{I}, s\rangle = \langle \mathbf{CT}, s\rangle = \langle \mathbf{T}, \partial s\rangle = 0$. The inconsistency arises when s encircles at least on electrode, since in this case the current through s is nonzero in general (it has to be equal to the current flowing through the encircled electrodes).

To solve this problem, in [13, Sec. 4] (here adapted to the context of a stationary current conduction problem) the potentials have been defined as

$$\mathbf{I} = \mathbf{CT} + \sum_{i=1}^{N_e} I_e^i \mathbf{\Pi}^i \tag{2}$$

where I_e^i is the current flowing through the ith electrode (which can be known if $\mathcal{E}_i$ is a current-driven electrode or unknown in the other case) and $\mathbf{\Pi}^i\}_{i=1}^{N_e}$ is the set of the so-called thick links. The formal definition of thick links involves a branch of algebraic topology known as cohomology theory [16] (Section II-D for a brief summary of the proposed definition and a survey of other approaches).

Concretely, each thick link is an array of integers, one integer for each face in $\mathcal{K}$. There is some freedom in choosing the integer coefficients of the ith thick link $\mathbf{\Pi}^i$, but they have to fulfill the following constraints [13]:

$$\mathbf{D}\,\mathbf{\Pi}^i = \mathbf{0} \tag{3}$$

$$\mathbf{E}_j \mathbf{\Pi}^i = \delta_{ij} \qquad \forall i, j \in \{1, \ldots, N_e\} \tag{4}$$

where the entries of the integer array $\mathbf{E}_j$ are

$$\begin{aligned} \langle \mathbf{E}_j, f\rangle &= 0 \qquad \forall f \notin \mathcal{E}_j \\ \langle \mathbf{E}_j, f\rangle &= \mathbf{D}(v, f) \qquad \forall f \in \mathcal{E}_j \end{aligned} \tag{5}$$

where $f \in \partial v$.

Intuitively, the simplest way to construct such a set of thick links is to consider the faces dual to oriented paths made by dual edges that connect the reference electrode to each other electrode. This idea, presented more rigorously and demonstrated in [13] by means of (co)homology theory, is the key of the efficiency of the novel algorithm presented in this paper in Section III-B.

To clarify the above statement, let us focus on the example represented in Fig. 2(a), where the three electrodes are represented by a thick line. A possible set $\{\mathbf{\Pi}^1, \mathbf{\Pi}^2\}$ of thick links is represented in Fig. 2(b) as thick black faces. In this picture, the paths made by dual edges are also shown. It is easy to realize that such thick links fulfill the two properties. Concerning the physical interpretation of the thick links, it is clear from (2) that the current evaluated on a 2-cycle which encircles the cavity is now constrained to be equal to the current through the cavity. The automatic construction of a set of thick links is the issue covered in Section III.

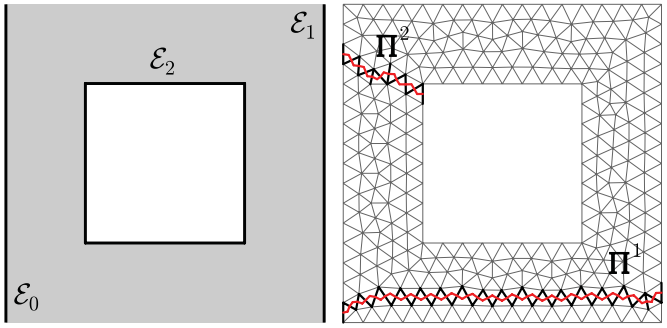

Fig. 2. (a) Example with three electrodes. (b) Set of thick links.

B. Construction of the Linear System of Equations

We introduce the resistance matrix $\mathbf{R}$ that relates the currents $\mathbf{I}$ to voltages $\tilde{\mathbf{U}}$ as

$$\tilde{\mathbf{U}} = \mathbf{RI}. \tag{6}$$

$\mathbf{R}$ is the discrete counterpart of the Ohm's constitutive law and can be efficiently computed as the FEM mass matrix generated from edge-element basis functions [11].

Finally, Faraday's discrete law

$$\tilde{\mathbf{C}}\tilde{\mathbf{U}} = \mathbf{0} \tag{7}$$

is enforced by a linear system of equations. By substituting (6) and (2) in (7), and recalling that $\tilde{\mathbf{C}} = \mathbf{C}^T$, an algebraic system of equations is obtained, as

$$\begin{aligned} \mathbf{C}^T\mathbf{RCT} + \sum_{j=1}^{N_v} \left(\mathbf{C}^T\mathbf{R}\mathbf{\Pi}^j\right) I_e^j \\ = -\sum_{k=N_v+1}^{N_e} \left(\mathbf{C}^T\mathbf{R}\mathbf{\Pi}^k\right) I_e^k \end{aligned} \tag{8}$$

where the electrodes $j \in \{1, \ldots, N_v\}$ are associated with a voltage constraint, while the others $k \in \{N_v + 1, \ldots, N_e\}$ are subject to a current constraint. We note that $\mathbf{C}^T\mathbf{RC}$ can be efficiently constructed as the nodal stiffness matrix [11].

The final algebraic linear system of equations contains one unknown $\mathbf{T}$ on all edges $e \in \mathcal{K}$ plus the unknown currents $\{I_e^j\}_{j=1}^{N_v}$. To close the linear system of equations, a set of nonlocal Faraday's laws [13] has to be added, one for each additional unknown, to specify the voltage on these electrodes with respect to the reference electrode. The nonlocal Faraday's laws are written on each thick link as

$$\mathbf{\Pi}^{iT}\tilde{\mathbf{U}} = U_e^i, \quad i \in \{1, \ldots, N_v\}.$$

By using (6) and (2), they can be written in terms of unknowns as

$$\begin{aligned} \left(\mathbf{\Pi}^{iT}\mathbf{RC}\right)\mathbf{T} + \sum_{j=1}^{N_v} \left(\mathbf{\Pi}^{iT}\mathbf{R}\mathbf{\Pi}^j\right) I_e^j \\ = U_e^i - \sum_{k=N_v+1}^{N_e} \left(\mathbf{\Pi}^{iT}\mathbf{R}\mathbf{\Pi}^k\right) I_e^k. \end{aligned} \tag{9}$$

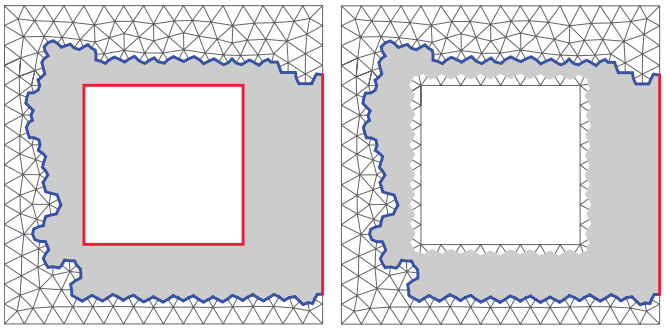

Fig. 3. (a) Cavity as the boundary of a perfect conductor. (b) Cavity as the boundary of a perfect insulator.

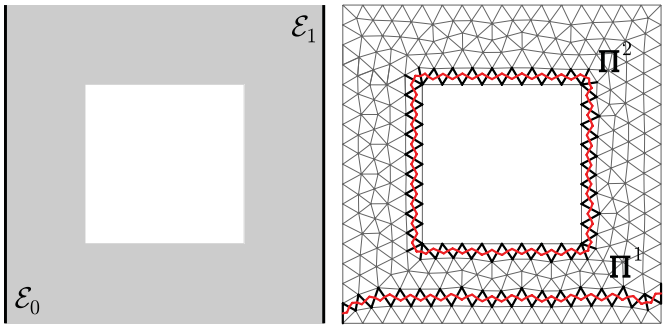

Fig. 4. (a) Example with two electrodes and a cavity which models a perfect insulator. (b) Set of thick links.

Let us call the (open) subcomplex of the elements belonging to $\bigcup_{i=0}^{N_e} \text{int}(\mathcal{E}_i)$ as $\mathcal{D}$. The complement with respect to $\partial\mathcal{K}$ is a closed subcomplex called $\mathcal{N}$. The homogeneous Neumann boundary condition is simply obtained by imposing the vector potential $\langle \mathbf{T}, e \rangle$ to be zero on each edge e belonging to $\mathcal{N}$, in such a way that the current associated to faces belonging to $\mathcal{N}$ is zero. A Dirichlet boundary condition is implicitly imposed by considering the vector potential $\mathbf{T}$ unknown on each edge e belonging to the considered boundary surface and writing the corresponding equation in (8) [13].

C. Cavities Formed by Perfect Insulators

The typical situation in electrostatics [13] is that all mesh cavities are boundaries of conductors, i.e., a Dirichlet boundary condition has to be enforced on them. Here we generalize the potential design to stationary conduction by considering also cavities made by perfect insulators, i.e., cavities whose boundaries are subject to a homogeneous Neumann boundary condition. In this case, cohomology theory tells us that there are additional thick links to consider.

Let us see the physical reason by considering again the example in Fig. 2(a). In this case, as one can easily realize by looking at Fig. 3(a), by adding up local Faraday's laws (7) one can deduce that the voltage on the dual path in the figure is zero (as it should be, since both its ends of the path lie on the same electrode).

We consider now another example in which only two electrodes are present and the cavity this time represents

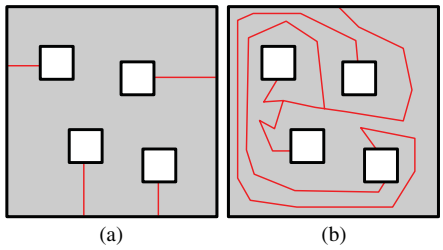

Fig. 5. (a) Thick links obtained by using the shortest path approach. (b) Thick links that may be obtained by the algorithm in [21].

the boundary of a perfect insulator [Fig. 4(a)]. Since local Faraday's laws are not written for edges belonging to $\mathcal{N}$ (the vector potential is enforced to zero instead), the voltage on the dual path cannot be deduced by summing up local Faraday's laws [Fig. 3(b)]. This implies that an additional link is needed to enforce the correct voltage and obtain the correct solution. The thick link has to encircle the cavity [$\mathbf{\Pi}^2$ in Fig. 4(b)], and the voltage on this additional link has to be imposed to zero.

Taking into account what was just stated, in general the potentials are defined as

$$\mathbf{I} = \mathbf{C}\mathbf{T} + \sum_{i=1}^{N_e} I_e^i \mathbf{\Pi}^i + \sum_{h=N_e+1}^{N_e+N_a} I_e^h \mathbf{\Pi}^h \tag{10}$$

where $\mathbf{\Pi}^h$ are the additional N_a thick links and I_e^h are the currents corresponding to the additional thick links. The linear system is easily obtained by following again the process of deducing (8) and (9).

D. Difference With Previous Approaches

In [10], thick links are defined as generators of the second de Rham cohomology group $H^2(\mathcal{K}, \mathbb{R})$. This definition implies that the electrodes on the boundary are treated differently with respect to interior electrodes. Electrodes on the boundary, in fact, are taken into account by applying inhomogeneous Dirichlet boundary conditions on $\mathbf{T}$ on each connected component of $\mathcal{N}$.

In this paper, thick links are defined as generators of $H^2(\mathcal{K} - \mathcal{N}, \mathbb{Z})$ [13]. First of all, we note that cohomology with integer coefficients is employed in place of the continuous de Rham theory [10], [19]–[20]. The second point is that electrodes placed in the interior of the domain and on the boundary are treated exactly in the same way. Apart from making the code and the exposition simpler, the definition used in this paper can be directly extended to 3-D problems [13] (while [10] cannot).

III. Thick Links Computation

A. Literature Survey

The generation of thick links has been discussed in some papers. In [12], no algorithm for thick link generation has been reported. In [10], thick links are computed as described in [21]. The algorithm is based on inflating an acyclic subcomplex in $\mathcal{K}$. At the end of this process, the faces belonging to the complement of the acyclic subcomplex are the support of

the union of all thick links. Each thick link is extracted from the support by finding paths between pairs of electrodes. This is not straightforward, since not all paths should be added but just a set of independent ones. The details of this procedure are not described in [10] or [21]. This algorithm is not attractive also because the thick links are in most cases far from being optimal, since their support is not minimal and they intersect frequently, see Fig. 5. We would like to mention that methods employing a standard computation of (co)homology generators [22] are not attractive because of the huge computational effort required. In [13], the author proposed a linear complexity algorithm based on the generalized spanning tree technique and another one based on the Dijkstra shortest path algorithm [23], whose worst-case complexity is $O(E + N \log N)$ with the most sophisticated implementation based on a Fibonacci heap [23].

B. Breadth-First Search-Based Algorithm

A new algorithm to automatically generate the thick links is now presented. The algorithm does not require any intervention of the user and it is easy to implement being based on the solution of the graph-theoretic shortest path problem [13]. The proposed algorithm has the virtue of producing an optimal set of thick links, and its worst-case complexity is linear with the number of elements in the mesh. By a set of optimal thick links we mean the set of thick links with the minimum support, which ensures that the fill-in of the sparse matrix of the linear system of equations is minimized. The algorithm, based on a breadth-first search (BFS) [23] single-source shortest path algorithm executed on an undirected and unweighted graph, is presented in Algorithm 1.

From lines 4 to 7 of Algorithm 1, the elements of $\mathcal{K}$ that touch $\mathcal{E}_0$ with at least one edge are enqueued and their distance to $\mathcal{E}_0$ is set to zero. From lines 8 to 19, the distances of the other triangles in $\mathcal{K}$ are found by using a BFS algorithm [23]. The propagation stops when all the electrodes are reached. The paths from each conductor boundary that define the thick links are easily found from lines 20 to 32 by using the predecessor information. The integer edge coefficients of the thick links are found by enforcing the discrete continuity law on each element, in such a way that (3) is ensured. Constraints (4) are also satisfied since each link intersects the corresponding electrode in just one face f_k (the end of the path starting from the reference electrode) and the thick link coefficient relative to f_k is set to the incidence $\mathbf{D}(v_j, f_k)$ at line 17, where v_j is the cell that contains f_k in its boundary. Moreover, the thick link relative to the ith electrode cannot intersect the jth electrode $\mathcal{E}_j$, with $i \neq j$, in one or more faces since only faces between two triangles are considered during the path retrieval (at least until the path reaches $\mathcal{E}_0$).

It is straightforward to see that, if the number of conductors is bounded by a constant $O(1)$, as it happens always in practice, then the worst-case computational complexity of the algorithm is linear w.r.t. the cardinality of the complex $\mathcal{K}$. This is due to the fact that each triangle of the mesh is considered at most two times during distance field computation (from lines 4 to 19), and at most N_v times during thick links retrieval (from lines 8 to 19). A more rigorous analysis of the BFS shortest path algorithm is given in [23].

Using this technique, the time required to generate thick links is so limited that it is negligible compared to the time needed by the rest of the simulation, i.e., the linear system solution. This is not the case when thick links are computed by a standard (co)homology computation [22]. We also note

Algorithm 1 2-D_Optimal_Thick_Links_Generation

1: integer $E \times N_v$ matrix thick_links;
2: vector of T integers distance initially set to ∞. distance[i] indicates the distance of the i-th triangle T_i with respect to $\partial\mathcal{K}$;
3: vector of T integers path. path[i] indicates the triangle from which T_i is discovered;
4: **for** $i = 1$ to T **do**
5: **if** some of the edges of T_i belong to $\mathcal{E}_0$ **then**
6: distance[i] $\leftarrow 0$;
7: queue $Q \leftarrow T_i$;
8: **while** Q is not empty **do**
9: triangle $T_p \leftarrow \text{pop}(Q)$;
10: **for** all triangles T_j that share an edge $\{E_i\}_{i=1}^{E}$ with T_p **do**
11: **if** distance[j] $= \infty$ **then**
12: distance[j] $\leftarrow$ distance[p] $+ 1$;
13: path[j] $\leftarrow T_p$;
14: $Q \leftarrow T_j$;
15: **if** T_j has an edge $E_k \in \partial\mathcal{E}_n$, $n \in \{1, \ldots, N_v\}$, and destination[n] $= 0$ **then**
16: destination[n] $\leftarrow T_j$;
17: thick_links[k, n] $\leftarrow \mathbf{D}(v_j, f_k)$, where $v_j \in \mathcal{K}$ corresponds to mesh triangle T_j and face $f_k \in \mathcal{K}$ to mesh edge E_k;
18: **if** destination[n] $\neq 0, \forall n \in \{1, \ldots, N_v\}$ **then**
19: break;
20: **for** $n = 1$ to N_v **do**
21: $T_i \leftarrow$ destination[n];
22: **while** true **do**
23: **if** distance[i] $= 0$ **then**
24: $d_i \leftarrow \mathbf{D}(v_i, :) \cdot$ thick_links[:,n], where $v_i \in \mathcal{K}$ correspond to the mesh triangle T_i;
25: thick_links[k, n] $\leftarrow -d_i\, \mathbf{D}(v_i, f_k)$, where E_k, corresponding to $f_k \in \mathcal{K}$, is the mesh edge of T_i on $\mathcal{E}_0$;
26: break;
27: **else**
28: $T_j \leftarrow$ path[i];
29: $E_k \leftarrow$ common edge between triangles T_i and T_j;
30: $d_i \leftarrow \mathbf{D}(v_i, :) \cdot$ thick_links[:, n], where $v_i \in \mathcal{K}$ correspond to the mesh triangle T_i;;
31: thick_links[k, n] $\leftarrow -d_i\, \mathbf{D}(v_i, f_k)$, where, as usual, $v_i \in \mathcal{K}$ corresponds to mesh triangle T_i and face $f_k \in \mathcal{K}$ to mesh edge E_k;
32: $T_i \leftarrow T_j$;
33: **return** thick_links;

Algorithm 2 2-D_Additional_Link_Generation

integer $E \times N_a$ matrix additional_thick_links representing the additional thick links;
for $E_i = 1$ to E **do**
  for each cavity $\mathcal{E}_c$ modeling a perfect insulator **do**
    $(n_1, n_2) \leftarrow$ nodes in the boundary of E_i (corresponding to face f_i) with $n_1 < n_2$;
    if $n_1 \in \mathcal{E}_c$ and $n_2 \notin \mathcal{E}_c$ **then**
      additional_thick_links$[f_i, c] \leftarrow 1$;
    if $n_2 \in \mathcal{E}_c$ and $n_1 \notin \mathcal{E}_c$ **then**
      additional_thick_links$[f_i, c] \leftarrow -1$;
return additional_thick_links;

that this algorithm may be directly extended to an arbitrary polygonal mesh, replacing triangles by a general 2-cell, or to 3-D polyhedral meshes, by considering paths made by dual edges on the 3-D cell complex.

C. Generation of the Additional Links

The fastest and simpler method of generating the additional links is to simply select as support the edges of the mesh $\{E_i\}$ that have one and only one boundary node belonging to the cavity $\mathcal{E}_c$ of the considered perfect insulator. Then, one has to orient them in such a way that all dual edges belonging to the dual cycle are iso-oriented. Since the orientation of mesh edges is assumed from the node with smallest label to the one with a higher label, this is simply performed by testing whether the node on $\mathcal{E}_c$ is the first one defining the edge or not. Then, the value $+1$ is assigned in the first case, and -1 otherwise, see Algorithm 2. It is straightforward to see, since each edge is considered at most one time, that the algorithm exhibits linear complexity.

A simple algorithm to automatically detect cavities that deserve this special treatment is also implemented. The first step of this algorithm is to find the connected components of the edges in the boundary of the mesh that belong to $\mathcal{N}$. This may be easily obtained again by a BFS algorithm [23]. Then, simply by testing whether the number of edges of the connected component is equal to the number of nodes of the connected component less 1, it is possible to determine whether the considered connected component forms a tree or it contains a cycle. If it contains a cycle, it needs the additional thick link constructed with Algorithm 2.

IV. Numerical Results

The algorithms described above have been integrated into the CDICE research code [24] implemented in Fortran 90. To solve the multiright-hand side sparse linear system of equations, the PARDISO direct solver contained in the Intel MKL scientific library has been employed. The hardware used for the computations consists of an Intel Core 2 Duo T7700 2.4-GHz laptop with 4 GB of RAM.

Four extraction techniques are compared: 1) the standard FEM formulation based on the scalar potential denoted as **V**; 2) the standard FEM formulation based on the scalar potential with second-order basis functions denoted as **V** 2nd order; 3) the original formulation presented in this paper using the vector potential denoted as **T**; and 4) the exploitation of complementarity by averaging the two solutions obtained by the **V** and **T** formulations previously introduced, referred to as $\mathbf{V} + \mathbf{T}$.

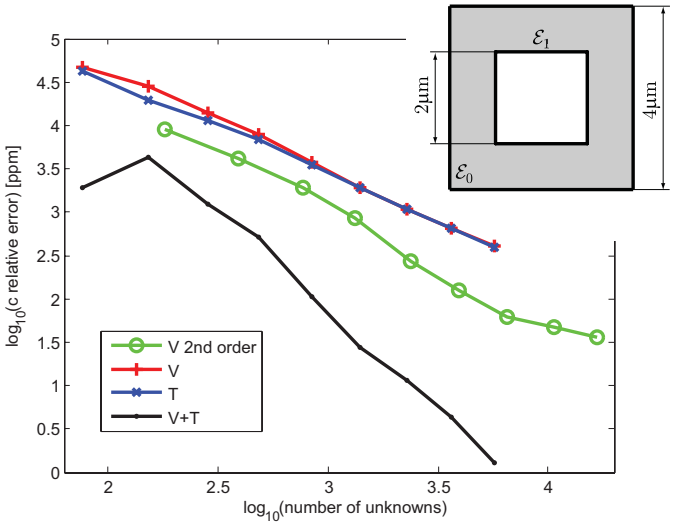

Fig. 6. Convergence of the p.u.l. capacitance value with respect to an increasing number of mesh elements for the square capacitor benchmark.

We note that the major novelty of using complementarity is that the exact values of the parameters lie inside the interval determined by the parameter estimations provided by the **V** and **T** formulations. Moreover, a high-quality error estimation for adaptive mesh refinement may be obtained easily by minimizing the so-called constitutive error [8]. Therefore, one can safely stop the mesh refinement (and the simulations) once the difference between the results obtained by the **V** and **T** formulations is smaller than a used-defined tolerance.

Four benchmarks are used to compare the extraction techniques in terms of speed and accuracy. First, the codes are validated by computing the capacitance of a simple square capacitor. Then, the results on a simple MTL parameter extraction problem that is frequently used in the literature as a benchmark are compared with those appearing in previous papers. Finally, a simple test case comprising a perfectly insulating cavity and a more complicated VLSI benchmark with floating dummy fills have been considered.

We remark as of now that, in all tested benchmarks, the time spent by Algorithms 1 and 2 for the potential design is negligible compared to the time required by the rest of the simulation.

A. Validation With a Square Capacitor

The code validation is performed by computing the p.u.l. capacitance of a square capacitor [25, p. 71] (Fig. 6). In Fig. 6, it is also shown how the p.u.l. capacitance value converges to the exact solution ($c_{\text{ref}} = 10.23409256\varepsilon_0$) when the number of elements is adaptively increased [8]. The logarithm to the base 10 of the relative error is considered in Fig. 6. It has been also verified that the results relative to the scalar potential (**V**) and to the vector potential (**T**) formulations provide, respectively,

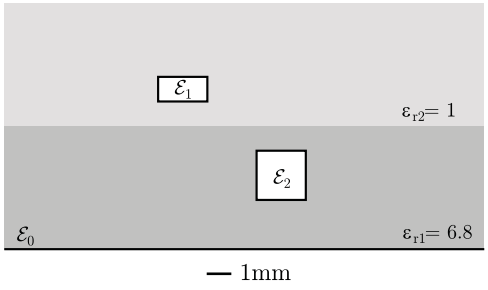

Fig. 7. MTL benchmark.

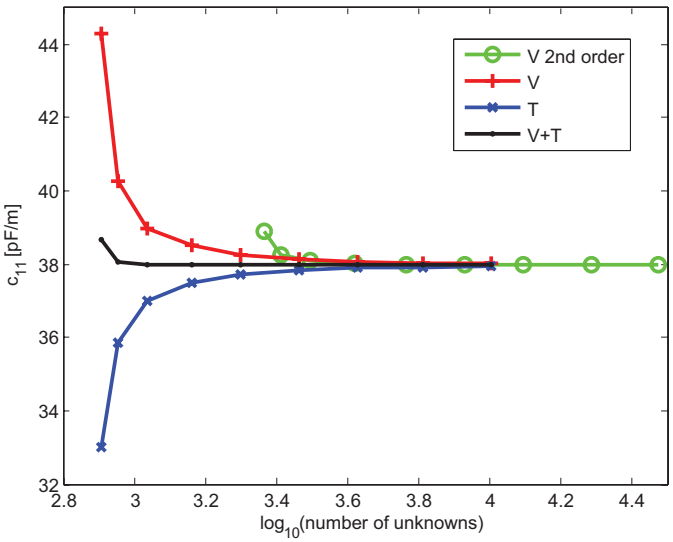

Fig. 8. Convergence of the c_{11} p.u.l. capacitance value with respect to an increasing number of mesh elements for the MTL benchmark.

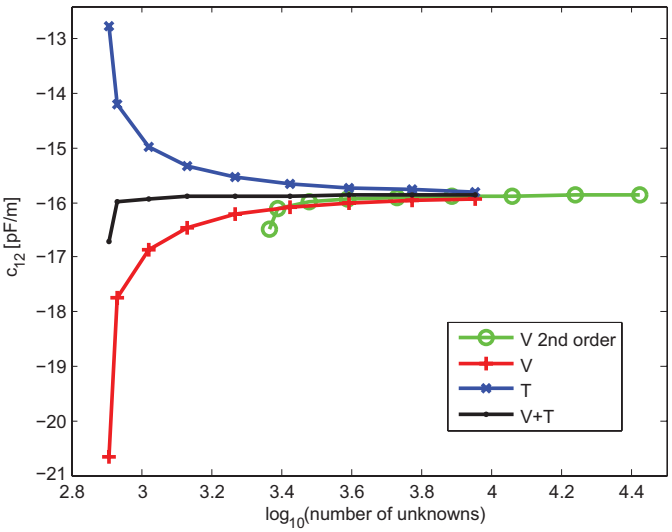

Fig. 9. Convergence of the c_{12} p.u.l. capacitance value with respect to an increasing number of mesh elements for the MTL benchmark.

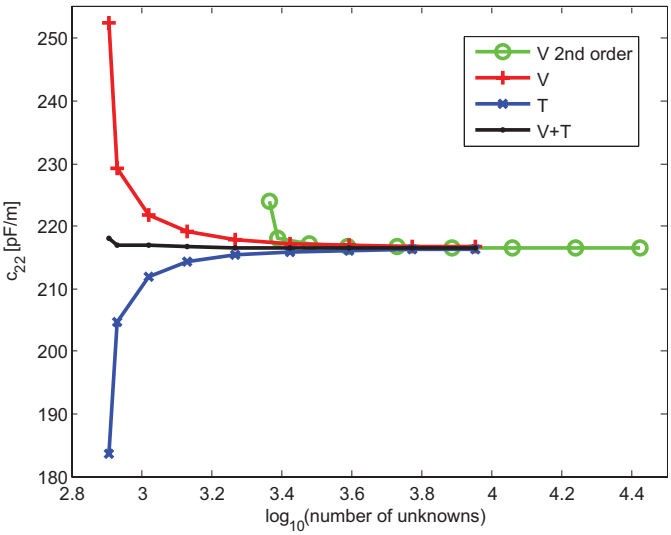

Fig. 10. Convergence of the c_{22} p.u.l. capacitance value with respect to an increasing number of mesh elements for the MTL benchmark.

the upper and lower bounds for the p.u.l. capacitance [4]. We also note that the mean value of the results provided by the two formulations, indicated as $(\mathbf{V}+\mathbf{T})$ in Fig. 6, produces a better estimate than first- or second-order FEM formulations based on the scalar potential. In particular, on the finest mesh with 5000 nodes, complementarity gives a relative error of 1.3 parts per million (ppm) in 0.46 s, while the relative errors obtained with first- and second-order FEM are 401 and 36.5 ppm in 0.23 and 0.67 s, respectively. This means a speedup for a given accuracy of more than one order of magnitude with respect to second-order FEM and even more with respect to the first-order FEM.

B. MTL Capacitance Extraction Benchmark

A benchmark for the extraction of MTL p.u.l. capacitance matrix proposed in [26] has been considered. The benchmark consists in two conductors in two different dielectric layers above a ground plane (Fig. 7). This benchmark has been frequently used in the literature for testing novel extraction techniques, see for example [27]–[30]. The convergence with mesh refinement of the elements of the MTL capacitance matrix are shown in Figs. 8–10. As one can see from these figures, the $\mathbf{V}+\mathbf{T}$ technique gives already after the third refinement a good parameter estimation. Moreover, the results obtained with the $\mathbf{V}$ and the $\mathbf{T}$ formulations define the tolerance intervals in which the exact value of the parameter has to lie. Refining the mesh reduces the extent of the confidence interval in such a way that the refinement may be safely stopped once the user-defined tolerance is reached. Table I contains the comparison of the capacitance values appearing in the literature and the ones obtained by the first- and second-order $\mathbf{V}$ FEM formulations, the $\mathbf{T}$ formulation, and with complementarity together with the simulation timings. The results obtained in the literature are not in as good an agreement as the ones provided by this paper. We remark that in the column relative to the results obtained by complementarity, not only one has a good estimate of the capacitance values but also guaranteed tolerance intervals.

C. Modeling Substrate Losses

The p.u.l. conductance is extracted for the configuration in Fig. 11 representing a portion of a substrate with two layers

TABLE I
CAPACITANCE MATRIX VALUES FOR THE MTL BENCHMARK

	[26]	[27] FEM	[27] MOM	[28]	[29]	[30]	CDICE **V**	CDICE **V** (Second-Order)	CDICE **T**	CDICE **V** + **T**
c_{11} [pF/m]	36.51	36.54	36.51	37.79	35.21	36.40	38.015	37.984	37.950	37.983 ± 0.033
c_{12} [pF/m]	−15.62	−15.38	−15.62	−15.71	−15.50	−15.80	−15.925	−15.864	−15.797	−15.861 ± 0.064
c_{22} [pF/m]	209.9	214.6	209.9	215.1	206.4	207.8	216.688	216.555	216.403	216.545 ± 0.142
Time [ms]	-	-	-	-	-	-	219	797	281	500

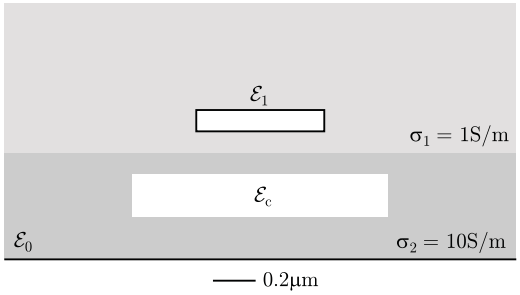

Fig. 11. Lossy substrate with a buried oxide benchmark.

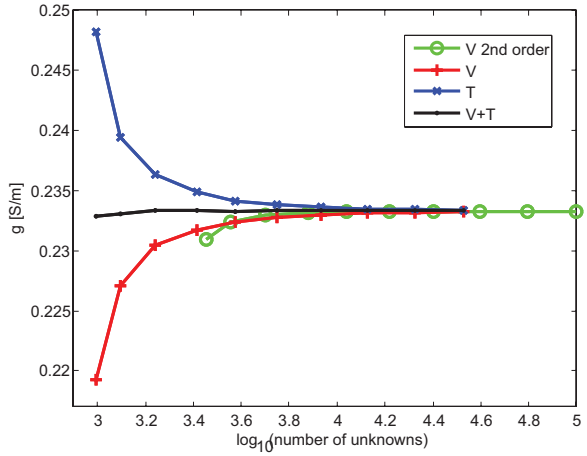

Fig. 12. Convergence of the p.u.l. conductance with respect to an increasing number of mesh elements for the lossy substrate with a buried oxide benchmark.

with heterogeneous material over a ground plane $\mathcal{E}_0$. A pad $\mathcal{E}_1$ is present together with a buried oxide cavity $\mathcal{E}_c$. First of all, it has been verified that the additional thick link introduced in this paper is necessary to get a correct solution with the vector potential formulation because of the presence of the insulating cavity. The convergence of the p.u.l. conductance g between $\mathcal{E}_1$ and $\mathcal{E}_0$ with mesh refinement is represented in Fig. 12. Again, with the third adaptive step, the estimation is already very good for the complementarity-based solver.

D. VLSI Capacitance Extraction With Dummy Fills

The presence of floating dummy fills may have a significant impact on the values of interconnect capacitances. As a final benchmark, we consider 3 active conductors and 24 floating dummy fills embedded in a five-layer dielectric (Fig. 13 for geometry and relative electric permittivity). The obtained self-capacitance c_{11} of $\mathcal{C}_1$ and the mutual capacitances c_{12}, c_{13} between $\mathcal{C}_1$ and $\mathcal{C}_2, \mathcal{C}_3$ are shown in Table II. Fig. 14 represents

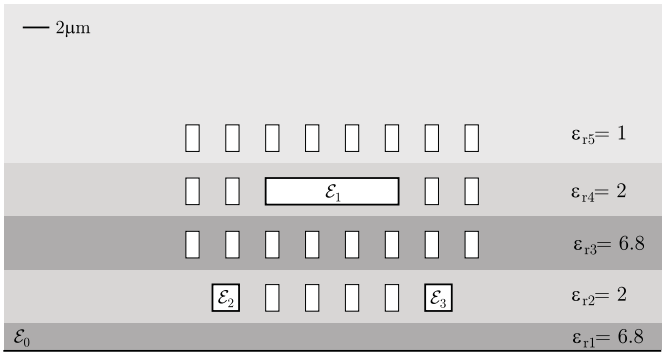

Fig. 13. Geometry of the VLSI capacitance extraction benchmark with dummy fills.

TABLE II
SELF- AND MUTUAL CAPACITANCES OF CONDUCTOR $\mathcal{C}_1$ IN THE VLSI BENCHMARK OBTAINED WITH CDICE

	V	**V** (Second-Order)	**T**	**V** + **T**
c_{11} [pF/m]	39.931	39.892	39.842	39.887 ± 0.045
c_{12} [pF/m]	−9.175	−9.162	−9.145	−9.160 ± 0.015
c_{13} [pF/m]	−9.175	−9.162	−9.145	−9.160 ± 0.015
Time [ms]	1203	5984	1328	2531

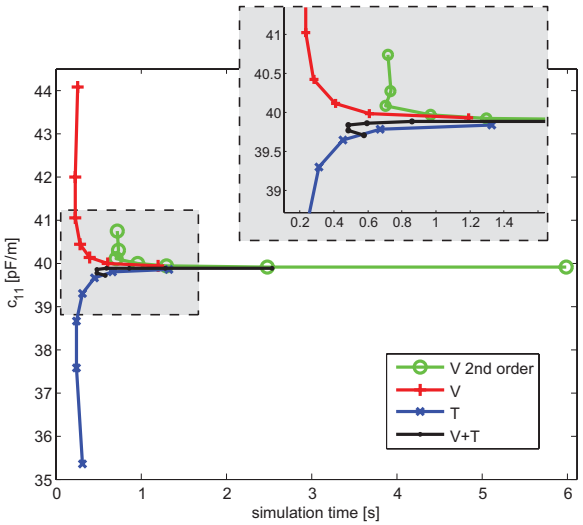

Fig. 14. Convergence of c_{11} with respect to simulation time for the VLSI benchmark. A zoom on the outlined region is also provided.

the c_{11} estimations with respect to simulation time for all the tested techniques. As in all the tested benchmarks, three or four adaptive mesh refinement steps are usually enough for complementarity to obtain sharp intervals where the capacitance values have to belong to. The same accuracy may be

obtained by the other formulations in at least one order of magnitude more time.

V. Conclusion

A pair of 2-D complementary formulations was applied for the numerical evaluation of the p.u.l. parameters of MTL. An efficient and general algorithm for the generation of thick links needed by the vector potential formulation was proposed, which has the virtue to be optimal in terms of speed and quality of the thick links obtained. Thanks to the technique proposed in this paper, complementarity is easy to implement in all FEM-based numerical codes and compares quite favorably with the standard first- and second-order FEM formulation based on the electric scalar potential only.

We found that the major advantage of using complementarity is that the exact values of the circuit parameters lie inside the tolerance intervals determined by the parameter estimations provided by **V** and **T** formulations. It was also verified that the mean of the two estimations gives good accuracy even with extremely coarse meshes. Finally, complementarity allows obtaining a high-quality adaptive mesh refinement, and one can safely stop the mesh refinement once the difference between the results obtained by the **V** and **T** formulations is smaller than the used-defined tolerance, being sure that the exact value of the parameters lies in between them. We also stressed that the advantage of complementarity is even bigger than what appears by the timings provided in this paper, since both first- and second-order FEM formulations take advantage of the complementarity-based adaptive mesh refinement.

References

[1] C. R. Paul, *Analysis of Multiconductor Transmission Lines*. New York: Wiley, 2007.

[2] R. Shen, S. X.-D. Tan, J. Cui, W. Yu, Y. Cai, and G. Chen, "Variational capacitance extraction and modeling based on orthogonal polynomial method," *IEEE Trans. Very Large Scale Integr. (VLSI) Syst.*, vol. 18, no. 11, pp. 1556–1566, Nov. 2010.

[3] W. H. Kao, C.-Y. Lo, M. Basel, and R. Singh, "Parasitic extraction: Current state of the art and future trends," *Proc. IEEE*, vol. 89, no. 5, pp. 729–739, May 2001.

[4] J. L. Synge, *The Hypercircle in Mathematical Physics*. Cambridge, U.K.: Cambridge Univ. Press, 1957.

[5] A. M. Arthurs, *Complementary Variational Principles*. New York: Oxford Univ. Press, 1970.

[6] J. T. Oden and J. N. Reddy, "On dual-complementary variational principles in mathematical physics," *Int. J. Eng. Sci.*, vol. 12, no. 1, pp. 1–29, Jan. 1974.

[7] P. Hammond and J. Penman, "Calculation of inductance and capacitance by means of dual energy principles," *Proc. IEE*, vol. 123, no. 6, pp. 554–549, Jun. 1976.

[8] J. A. H. Rikabi, C. F. Bryant, and E. M. Freeman, "Complementary solutions of electrostatic field problems," *IEEE Trans. Magn.*, vol. 25, no. 6, pp. 4427–4442, Nov. 1989.

[9] J. A. H. Rikabi, "Complementary solutions of direct current flow problems," *IEEE Trans. Magn.*, vol. 29, no. 1, pp. 98–107, Jan. 1993.

[10] Z. Ren, "2-D dual finite-element formulations for the fast extraction of circuit parameters in VLSI," *IEEE Trans. Magn.*, vol. 39, no. 3, pp. 1590–1593, May 2003.

[11] J. Jin, *The Finite Element Method in Electromagnetics*. New York: Wiley, 2002.

[12] Z. Ren, "A 3D vector potential formulation using edge element for electrostatic field computation," *IEEE Trans. Magn.*, vol. 31, no. 3, pp. 1520–1523, May 1995.

[13] R. Specogna, "Complementary geometric formulations for electrostatics," *Int. J. Numer. Meth. Eng.*, vol. 86, no. 8, pp. 1041–1068, May 2011.

[14] M. Michelutti and R. Specogna, "RETICULA: A light, fast and flexible 2D triangular mesh generator for biomedical applications," to be published.

[15] E. Tonti, "A direct discrete formulation of field laws: The cell method," *Comput. Model. Eng. Sci.*, vol.2, no. 2, pp. 237–258, 2001.

[16] J. R. Munkres, *Elements of Algebraic Topology*. Cambridge, MA: Perseus Books, 1984.

[17] E. Tonti, "On the formal structure of physical theories," in *Monograph of the Italian National Research Council*. Milano, Italy: Istituto Di Matematica Del Politecnico Di Milano 1975.

[18] P. Dłotko, R. Specogna, and F. Trevisan, "Automatic generation of cuts on large-sized meshes for the T-Ω geometric eddy-current formulation," *Comput. Methods Appl. Mech. Eng.*, vol. 198, nos. 47–48, pp. 3765–3781, 2009.

[19] P. R. Kotiuga, "Hodge decompositions and computational electromagnetics," Ph.D. dissertation, Dept. Electr. Eng., Univ. McGill, Montreal, QC, Canada, 1985.

[20] P. W. Gross and P. R. Kotiuga, *Electromagnetic Theory and Computation: A Topological Approach*, (MSRI Monograph series), vol. 48. Cambridge, U.K.: Cambridge Univ. Press, 2004.

[21] Z. Ren and A. Razek, "Boundary edge elements and spanning tree technique in three-dimensional electromagnetic field computation," *Int. J. Numer. Meth. Eng.*, vol. 36, no. 17, 1993, pp. 2877–2893.

[22] P. Dłotko and R. Specogna, "Efficient cohomology computation for electromagnetic modeling," *Comput. Model. Eng. Sci.*, vol. 60, no. 3, pp. 247–278, 2010.

[23] T. H. Cormen, C. E. Leiserson, R. L. Rivest, and C. Stein, *Introduction to Algorithms*. Cambridge, MA: MIT Press, 2001.

[24] R. Specogna. (2012). *CDICE: Complementarity and Duality in Computational Science and Engineering* [Online]. Available: http://www.comphys.com/

[25] E. Durand, *Électrostatique Méthodes de Calcul, Diélectriques*. Paris, France: Masson, 1966.

[26] C. Wei, R. F. Harrington, J. R. Mautz, and T. K. Sarkar, "Multiconductor transmission lines in multilayered dielectric media," *IEEE Transmiss. Microw. Theory Tech.*, vol. 32, no. 4, pp. 439–445, Apr. 1984.

[27] R. L. Khan and G. I. Costache, "Finite element method applied to modeling crosstalk problems in printed circuit boards," *IEEE Trans. Electromagn. Compat.*, vol. 31, no. 1, pp. 5–15, Feb. 1989.

[28] G. Plaza, F. Mesa, and M. Horno, "Quick computation of [C], [L], [G], and [R] matrices of multiconductor and multilayered transmission systems," *IEEE Trans. Microw. Theory Tech.*, vol. 43, no. 7, pp. 1623–1626, Jul. 1995.

[29] A. Papachristoforos, "Method of lines for analysis of planar conductors with finite thickness," *IEE Proc. Microw. Antennas Propag.*, vol. 141, no. 3, pp. 223–228, Jun. 1994.

[30] W. Shu and S. Xu, "Capacitance extraction for multiconductor transmission lines in multilayered dielectric media using the numerical Green's function," *Microw. Opt. Technol. Lett.*, vol. 40, no. 6, pp. 529–531, 2004.

Ruben Specogna (S'05–M'08) was born in Cividale del Friuli (UD), Italy, in 1977. He received the Master's degree in electronic engineering and the Ph.D. degree in electrical engineering from the University of Udine, Udine, Italy, in 2003 and 2007, respectively.

He is an Assistant Professor of Electromagnetic Compatibility and Electrical Science in the University of Udine, Udine, Italy, in 2008. He is the author of more than 50 papers in ISI scientific journals, mainly in the field of computational electromagnetism, coupled problems (MEMS and nanoelectronics), computational topology and computer aided design, nuclear fusion reactors engineering and design, and biosensors.